

TETHERED HOVER FLIGHT TESTS OF BASELINE CONTROL LAWS FOR A TANDEM TILT-WING SUB-SCALE DEMONSTRATOR

Daniel Milz[1,2], Leo Ott[1] & Marc May[1,2]

[1]Institute of Flight Systems, German Aerospace Center (DLR), 82234 Weßling, Germany
[2]TUM School of Engineering and Design, 85521 Ottobrunn, Germany

Abstract

Flight control laws for tandem tilt-wing aircraft must account for complex mechanics and aerodynamic interactions. This complexity, along with the absence of proven control designs for these vehicles, necessitates rigorous validation of control strategies. Rapid prototyping sub-scale demonstrators have been shown to be a suitable intermediate step between simulative validation and full-scale flight testing. This paper presents the flight control design, test preparations, procedures, and results for the tandem tilt-wing sub-scale demonstrator *TANDEMIC*, a $15\,\mathrm{kg}$ modular testbed constructed with 3D-printed components, during its tethered maiden flights. The flight control system employs a baseline control design, serving as a fallback solution and reference for future, more advanced, controller tests. To ensure a safe testing environment, tethered hover flights are conducted, and the necessary adaptations to the flight control system are described. The experimental setup and test sequences are detailed, with emphasis on verifying the control laws in flight with disturbances and propulsion system vibrations within safe, constrained conditions. The results validate the applicability, closed-loop stability, and robustness of the baseline control system.

Keywords: Flight Control, Flight Testing, Tilt-Wing, eVTOL

1. Introduction

Electric Vertical Take-Off and Landing (eVTOL) aircraft are designed to enhance short- to medium-haul transportation. Tandem tilt-wing architectures offer a particularly advantageous design, providing a higher lift-to-drag ratio in cruise than multicopters and reduced mechanical complexity compared to tilt-rotors. However, these configurations introduce complex aerodynamic interactions and other mechanical challenges, especially during the transition phase. The transition corridor, defined as the flight regime between hover and wing-borne flight, is characterized by phenomena such as flow separation, propeller slipstream interactions, and tandem effects, which render linear control models inadequate [1, 2]. Realizing the potential of these aircraft depends on mastering the complex aerodynamics and flight dynamics inherent to the transition between vertical and horizontal flight.
Control of tilt-wing aircraft is complicated by nonlinear, unsteady aerodynamic phenomena encountered during transition, including separated flows and propeller slipstream effects. Although theoretical models guide control law development, physical validation remains essential. Airworthiness assurance requires a validation strategy that bridges the gap between simulation and free flight. High-fidelity computational fluid dynamics (CFD) and wind tunnel tests provide static stability data but cannot fully capture the dynamic coupling between the flight control system (FCS) and the unsteady aerodynamics of a maneuvering aircraft. Additionally, simulation-based validation and verification strategies inherently lack real-world effects. Therefore, sub-scale demonstrators have been proven to bridge this gap by allowing for flight dynamic validation and flight control law testing [3, 4]. To address this need, *TANDEMIC (Tilt-wing Aircraft for Novel Demonstrations of eVTOL Modeling and Innovative Control)*, a modular sub-scale demonstrator, was developed to validate control laws for the tandem tilt-wing configuration [5].

1.1 Historical and Contemporary Demonstrators

Scaled tilt-wing demonstrators have been used in research for several years. Especially relevant to this work are the developments undertaken at NASA Langley Research Center [3, 6, 4, 7] and the University of Oxford [8, 9], as their demonstrators resemble use cases, dimensions, and fabrication methods similar to those of this work.

NASA's GL-10 "Greased Lightning" (25.9 kg, 3.17 m wingspan) successfully demonstrated the transition using a distributed electric propulsion (DEP) system on a carbon-fiber airframe [3]. Its testing highlighted the importance of robust control during the post-stall regime of the wings during transition [3]. Following this, the NASA Langley Aerodrome No. 8 (LA-8) adopted a rapid prototyping philosophy, using a load-bearing carbon fiber structure with modular, 3D-printed aerodynamic shells [6]. This approach is also seen in their recent RAVEN-SWFT testbed (16.8 kg) [4, 7].

The University of Oxford has investigated a tilt-wing demonstrator of comparable size [8, 9]. They have also utilized tethered hover tests to validate control laws.

1.2 Flight Control Architectures

Controlling tilt-wing aircraft is challenging due to high nonlinearity, actuator saturation, and strong coupling between axes.

Traditional linear control methods require gain scheduling to cover the entire flight envelope and must cope with the rapidly changing plant dynamics of a tilting wing [1]. Consequently, Nonlinear Dynamic Inversion (NDI) has emerged as a preferred solution for decoupling the nonlinear dynamics.

NDI relies on an on-board model to invert the aircraft's nonlinear dynamics [10], thus making it sensitive to model mismatch. Further developments, including incremental and sensory NDI, replace model-based estimations with appropriate acceleration measurements. Thus, the susceptibility to model uncertainties is largely reduced by increasing the reliance on sensor measurements [11]. Recent research focuses on hybrid NDI, which blends model-based NDI (superior at high frequencies) with sensory NDI (superior at low frequencies) via a complementary filter. This approach allows for a trade-off between the two methods, effectively increasing the controller's robustness [1, 12].

However, all methods are to some extent sensitive to the on-board plant model and the sensor system, including delays and synchronization, as well as actuator properties. This makes flight control tests more challenging and motivates the use of tethered flight tests and a robust backup control system in case of instability.

1.3 Contribution of the paper

To enable safe testing and establish a baseline reference and fallback solution, this paper focuses on the design and validation of a robust baseline controller for the *TANDEMIC* sub-scale tandem tilt-wing demonstrator.

This study builds upon previous research on control design [1] and the validation and robustness analysis [13] of a hybrid NDI controller for a tandem tilt-wing eVTOL. The sub-scale demonstrator described in [5] is employed to test and validate the flight dynamics and control laws through flight tests. The focus is specifically on the initial tethered hover test campaign, which represents the first step toward free flight. The results validate the control law design, control allocation implementation, and disturbance rejection properties within a safe, constrained environment. In doing so, this work bridges the gap between theoretical control design and physical flight validation for tandem tilt-wing eVTOL aircraft, helps verify the test procedures and hardware, and the current flight dynamics model. Additionally, specific tethered phenomena, such as reduced envelope limits and tethering forces during constrained hover, are investigated. Mitigation strategies for the control laws are proposed and implemented. Subsequently, the approach and flight control laws are validated through hover flight tests under tethered conditions.

2. The *TANDEMIC* Sub-Scale Demonstrator

The *TANDEMIC* demonstrator [5] shown in Fig. 1 serves as the testbed for this research. This sub-scale tandem tilt-wing aircraft is designed according to rapid prototyping principles, balancing flight performance, robustness, modularity, and ease of repair. The aircraft features a wingspan of $1.5\,\mathrm{m}$ and a design take-off mass of $15\,\mathrm{kg}$. Its configuration includes two tandem wing pairs and a DEP system with eight propellers. Structurally, *TANDEMIC* employs a hybrid design strategy to optimize modularity and enable rapid iteration. The internal skeleton comprises carbon-fiber spars and laser-cut aluminum fuselage frames, providing structural integrity under critical loads, such as 3G maneuvers. Aerodynamic surfaces, including the wings and fuselage hull, are fabricated using a desktop 3D printer with variable-density foamed Acrylonitrile Styrene Acrylate (ASA) material [5]. The propulsion system consists of eight electric motors driving two-bladed propellers, achieving a thrust-to-weight ratio of approximately 2 [5]. Motor mounting segments are 3D-printed and reinforced to withstand significant off-axis moments and gyroscopic loads during tilting transitions [5]. The modular wing architecture enables rapid reconfiguration of motor positions and control surfaces, supporting iterative testing of various control allocation strategies.

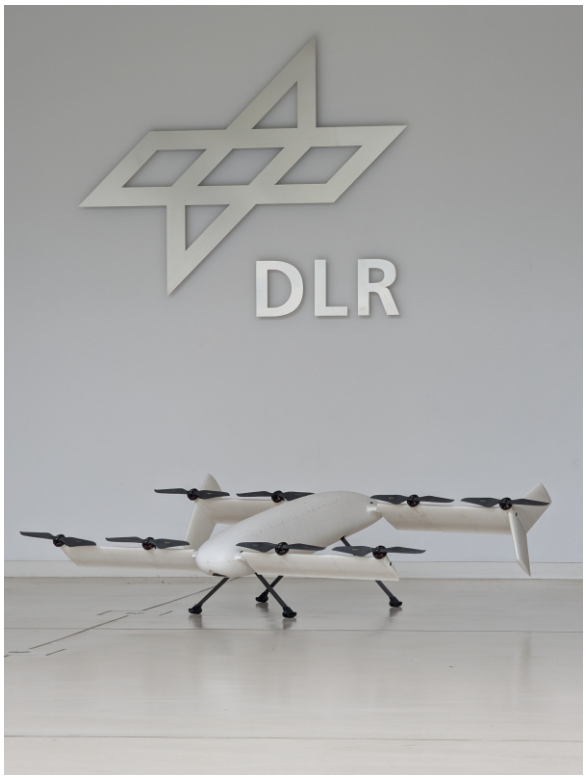


Figure 1 – *TANDEMIC* Sub-Scale Tilt-Wing Demonstrator

The flight control systems is developed in MATLAB/SIMULINK and implemented on a PIXHAWK 6X running the PX4 software stack.

2.1 Equations of Motion

The flight dynamics of the demonstrator are described by the nonlinear 6-DOF equations of motion. For hover and low-speed flight, the dynamics can be simplified by neglecting aerodynamic forces on the fuselage, as the vehicle is propulsion-dominated. The control inputs of the system are depicted in Fig. 2.

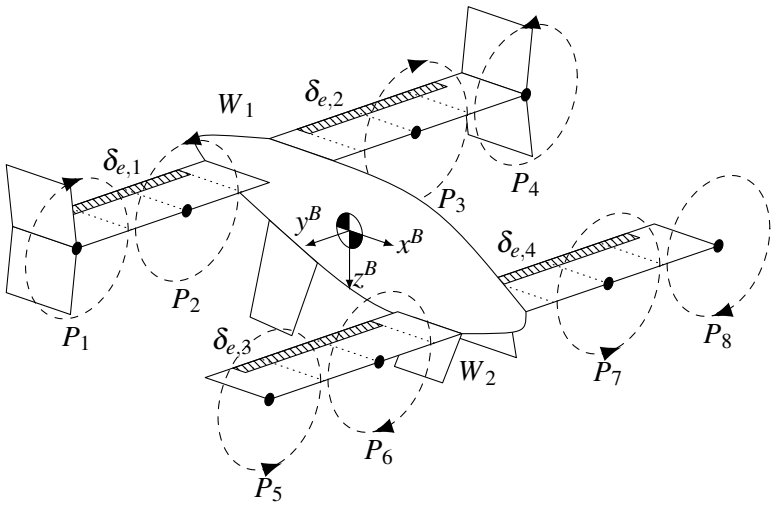


Figure 2 – 3D sketch of the tandem tilt-wing configuration.

The equations of motion are given by:

$$\dot{r} = \mathbf{R}_{NB}(\Theta)\ v^B, \tag{1a}$$

$$\dot{\Theta} = \mathbf{R}_{\Theta B}\ \omega^B, \tag{1b}$$

$$\dot{v}^B = v^B \times \omega^B + g + \frac{1}{m} f, \tag{1c}$$

$$\dot{\omega}^B = \mathbf{I}^{-1}\left(m - \omega^B \times \mathbf{I}\omega^B\right), \tag{1d}$$

where r is the position vector, Θ the attitude angles, v^B the body-frame velocity, ω^B the body-frame angular rates, m the mass, I the inertia matrix, and g the gravitational acceleration. The forces f and moments m are derived from the propeller thrust T_i and drag D_i, as well as control surface deflections $\delta_{e,i}$. See Fig. 2 for a precise assignment of the control inputs. The detailed aero-propulsive model is presented in [2, 13]. The main parameters of the sub-scale demonstrator are listed in Table 1.

Parameter	Symbol	Value
Mass	m	$15\,\mathrm{kg}$
Inertia matrix	$\mathbf{I}$	$\begin{bmatrix} 1.810 & -0.032 & -0.646 \\ -0.032 & 3.012 & -0.008 \\ -0.646 & -0.008 & 3.672 \end{bmatrix} \mathrm{kg\,m^2}$
Center of gravity	r^B_{cg}	$\begin{bmatrix} -0.590 & 0.00425 & -0.179 \end{bmatrix}^\top \mathrm{m}$
Wingspan	b	$1.5\,\mathrm{m}$
Wing area aft / front / total	S	$0.335\,\mathrm{m^2}$ / $0.237\,\mathrm{m^2}$ / $0.572\,\mathrm{m^2}$
Wing chord aft / front	$\bar{c}$	$0.215\,\mathrm{m}$ / $0.157\,\mathrm{m}$
Airfoil		GA(W)-1 (17 % thickness)
Thrust-to-weight-ratio	T/W	2
Hover endurance		10 min with 20 % reserve

Table 1 – Key parameters of the *TANDEMIC* sub-scale demonstrator [5].

2.2 Propulsion Model

During hover flight, the vehicle dynamics are propulsion-dominated. Furthermore, during hover flight, the operating point and advance ratio of the propellers change only slightly, allowing the assumption of a constant-coefficient model identified in ground tests. The thrust T_i and torque Q_i of each propeller are modeled according to:

$$T_i = C_T \rho A \left(\Omega_i R\right)^2, \tag{2a}$$

$$Q_i = C_Q \rho A \left(\Omega_i R\right)^2 R, \tag{2b}$$

where $C_T = 0.0859$ and $C_Q = 0.00516$ are the thrust and torque coefficients, ρ the air density, $A = \pi R^2$ the propeller disk area, Ω_i the propeller rotational speed, and $R = 0.202\,\mathrm{m}$ the propeller radius. Within the hover flight regime, the coefficients can be assumed nearly constant. However, for transition and cruise flight, the coefficients depend on the advance ratio of the propeller [13].

3. Flight Control Laws

The flight control system design for this configuration is shown in Fig. 3 and explained in detail in [1, 13]. The control design is carried out in MATLAB/SIMULINK and implemented on a HOLYBRO PIXHAWK 6X with PX4 firmware. In this work, the focus is on the baseline controller, which serves as a reference and backup for future tests of more advanced control functions. Furthermore, its simplicity helps validate the test setup and procedures, especially the hardware implementation, coding, and the setup of the PIXHAWK environment.

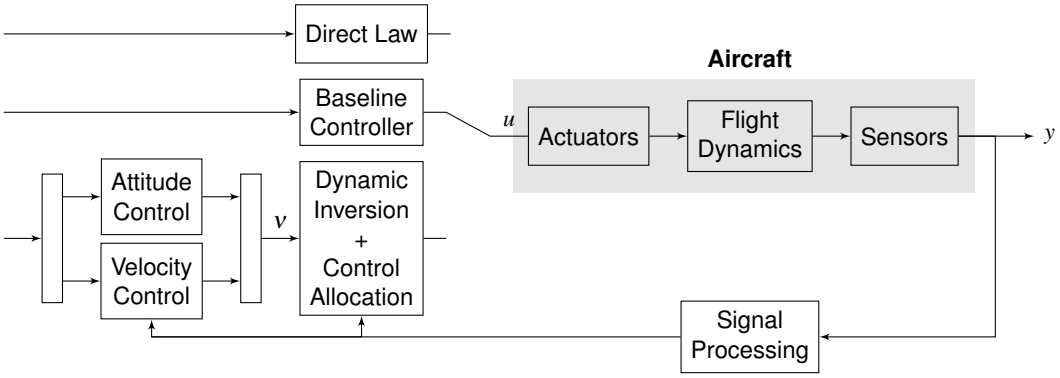


Figure 3 – Inner loop control architecture for the tandem tilt-wing control [1].

3.1 Considerations for Tethered Tests

Flight testing on a tether introduces specific dynamic artifacts that the control law must handle. The tether introduces external forces and moments not present in the internal flight model and, thereby, acts as a disturbance. When encountering limitations, this can be critical, as the controller might drive the system further beyond the limit and wind up. To counteract these mechanisms, integrator wind-up prevention is required as the aircraft may be physically unable to reach a target position or velocity due to the tether limits.

Pilot stick mapping To allow sufficient control during hover, the test pilot can command the velocities v_x, v_y, and v_z, as well as the yaw rate $\dot{\psi}$. The roll angle ϕ is controlled by v_y and the pitch angle θ by v_x. The commands are restricted to a maximum of $1\,\mathrm{m\,s^{-1}}$. Alternatively, the pilot can switch to attitude control mode and directly command the roll and pitch angles ϕ and θ, as well as the yaw rate $\dot{\psi}$. As a third alternative, the pilot can enable one additional cascade: the position controller. However, during indoor hover tests, position accuracy is often insufficient without an additional position-sensing setup. In all modes, the pilot commands the yaw rate $\dot{\psi}$, but the controller implements a Rate Command Attitude Hold (RCAH) logic, which tracks the resulting heading. Additionally, a pre-allocated direct law is available for testing.

Take-Off Another characteristic of tethered hover tests is the take-off transient. In our setup, the vehicle is initially suspended by the tether with the possibility to climb slightly until the lower tethers engage. The initial slack is around $0.5\,\mathrm{m}$. Thus, the take-off procedure must be performed smoothly. During take-off, it is important to ascend uniformly without adverse moments. This means that not only the propeller forces and moments, but also the slipstream-induced aero-propulsive forces and moments, need to be balanced until a force equilibrium is reached with the gravitational vector. When on the ground, the moments are counteracted by the ground force and only occur after take-off. However, the tethered vehicle already has its rotational degrees of freedom if some slack is present. Thus, moment control must be present during the buildup of force before lifting off. Conversely, this means the attitude has to be stabilized as well. In this take-off setup, the tether force f_t^B can be described as:

$$f_\mathrm{t}^B = mg - f_\mathrm{p}^B - f_\mathrm{a}^B \tag{3}$$

3.2 Baseline Hover Controller

To safely validate the mechanical tether setup described in Sec. 4. and mitigate risk during the maiden constrained hover tests, a robust baseline controller was implemented prior to testing more advanced, experimental flight control laws. Because the *TANDEMIC* demonstrator introduces complex coupled dynamics and the dual-tether system introduces unmodeled external forces, establishing a flight baseline with a proven, robust control strategy was essential. Furthermore, the baseline controller can be used as a fallback during untethered flight tests. The baseline controller uses a classical cascaded PID architecture. The baseline system manages the over-actuated system via a fixed

allocation matrix. This simplified approach guarantees deterministic actuator responses, enabling evaluation of the demonstrator's fundamental mechanical and structural stability in hover. Because external tether forces act as persistent disturbances that could cause integral saturation at a physical boundary, the baseline system incorporates mechanisms to prevent integral wind-up. This is done by limiting the integrators based on envelope limits, as all integrators can be interpreted physically. By utilizing this robust baseline controller, the experimental results in Sec. 5. demonstrate that the mechanical tether envelope functions safely and serves as a dynamic baseline. The proposed control architecture is shown in Fig. 4. The fixed control allocation is realized by the matrices shown in Fig. 4:

$$M_{p,xy} = \begin{bmatrix} -1 & -1 & 1 & 1 & -1 & -1 & 1 & 1 \\ -1 & -1 & -1 & -1 & 1 & 1 & 1 & 1 \end{bmatrix}^\top \qquad M_{p,\Sigma} = \begin{bmatrix} 1 & 1 & 1 & 1 & 1 & 1 & 1 & 1 \end{bmatrix}^\top$$

$$M_{p,z} = \begin{bmatrix} 1 & -1 & -1 & 1 & -1 & 1 & 1 & -1 \end{bmatrix}^\top \qquad M_{e,z} = \begin{bmatrix} 1 & 1 & 1 & 1 \end{bmatrix}^\top$$

The gains of the baseline controller were achieved through multi-objective optimization [13].

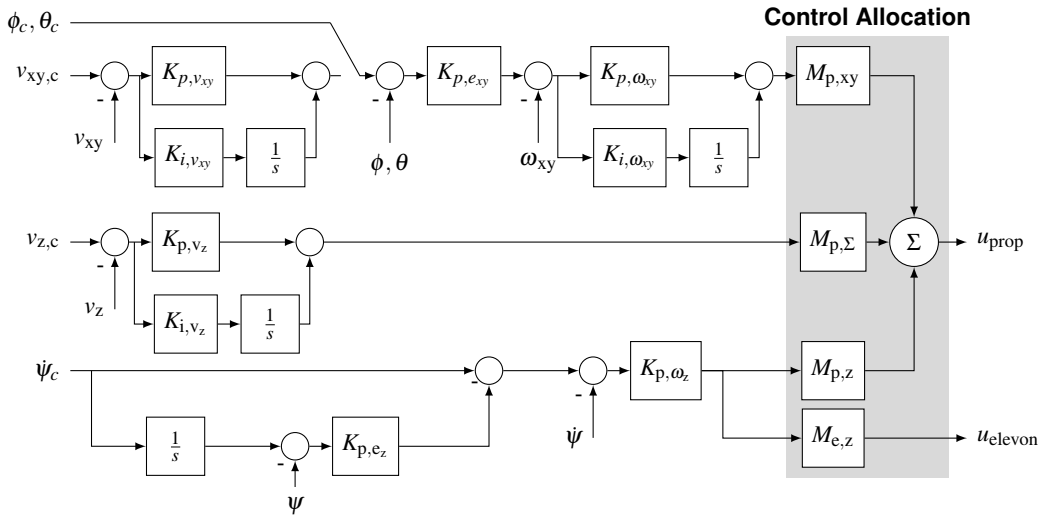


Figure 4 – Control architecture of the baseline hover controller.

3.3 Stability and Robustness

The stability and robustness of the control law are evaluated using disk margins [14] and μ-analysis. The description of the analysis process is presented in another publication [13]. Furthermore, the control parameter synthesis is performed using MOPS and optimizes the parameters in the worst case, obtained via a worst-case search [15]. The resulting controller has been shown to posses sufficient robustness according to the metrics from [13].

4. Test Setup and Preparations

The testing environment is designed to minimize risk while still allowing for sufficient dynamic validations. It is shown in Fig. 5.

4.1 Infrastructure

The tests are conducted in an indoor facility to eliminate wind disturbances. The aircraft is suspended from a gantry crane system. A dual-tether system (top and bottom) is used (see Fig. 6). All mounting points attach directly to the internal aluminum fuselage skeleton [5]. Static cut-resistant Kevlar tethers were used, fitted with 3D-printed elastomer dampers sized to limit the peak load when a tether is engaged.



Figure 5 – Tethered hover flight test setup.

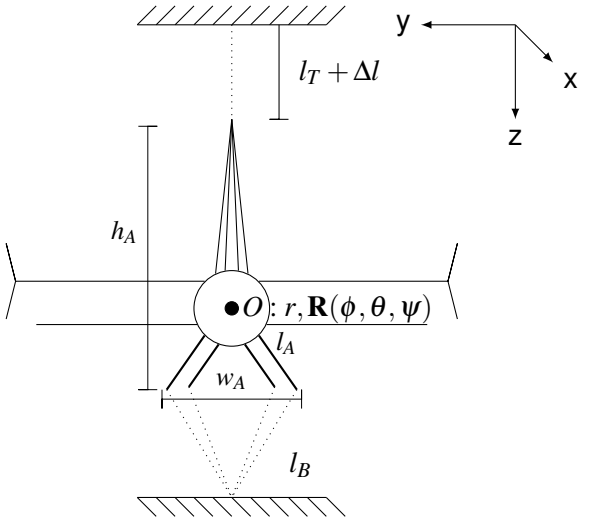


Figure 6 – Tethered test rig: rigid structure in solid (——) and ropes in dotted lines (·····).

Top rope length	l_T	3 m
Bottom rope length	l_B	3.5 m
CG to top tether mount	h_T	1.0 m
CG to bottom tether mount	h_B	0.36 m
Distance between leg tips	w_A	0.4 m
CG to legs tips	l_A	0.8 m

Table 2 – Parameters of the tethered test rig setup.

4.2 Operational Envelope

The setup is designed to restrict the envelope, thereby securing the aircraft. By lowering the aircraft with the crane, the aircraft's envelope increases. Figure 6 shows the mechanical setup.
The envelope, i.e., the deviation from the zero point O as translational $r = [\Delta x, \Delta y, \Delta z]$ and rotational $\mathbf{R}(\phi, \theta, \psi)$ deviations, depends on the play of the top rope Δl and is defined by the constraints

$$\textbf{1 top constraint:} \quad \left\| r + \mathbf{R}(\phi,\theta,\psi) \begin{bmatrix} 0 \\ 0 \\ -h_T \end{bmatrix} - \begin{bmatrix} 0 \\ 0 \\ -h_T - l_T \end{bmatrix} \right\|_2 \leq l_T + \Delta l \tag{4a}$$

$$\textbf{4 bottom constraints:} \quad \left\| r + \mathbf{R}(\phi,\theta,\psi) \begin{bmatrix} \pm\frac{l_A}{2} \\ \pm\frac{w_A}{2} \\ h_B \end{bmatrix} - \begin{bmatrix} 0 \\ 0 \\ \sqrt{l_B^2 + \frac{l_A^2 + w_A^2 + 4h_B^2}{4}} \end{bmatrix} \right\|_2 \leq l_B \tag{4b}$$

where ψ is free and can be neglected due to the joints. Figure 7 shows the envelope limits for all axis-at-a-time deviations. With this setup we can establish a safe flight envelope for hovering, while ensuring that the tethers stay clear of the propellers in every possible attitude.

4.3 Hardware-in-the-Loop (HIL)

Prior to the tethered hover tests, the controllers underwent a validation campaign. The controller was first deployed to the PIXHAWK 6X flight control computer running the PX4 firmware stack in a Hardware-in-the-Loop (HIL) simulation, utilizing a MAVLINK bridge to exchange synthetic sensor

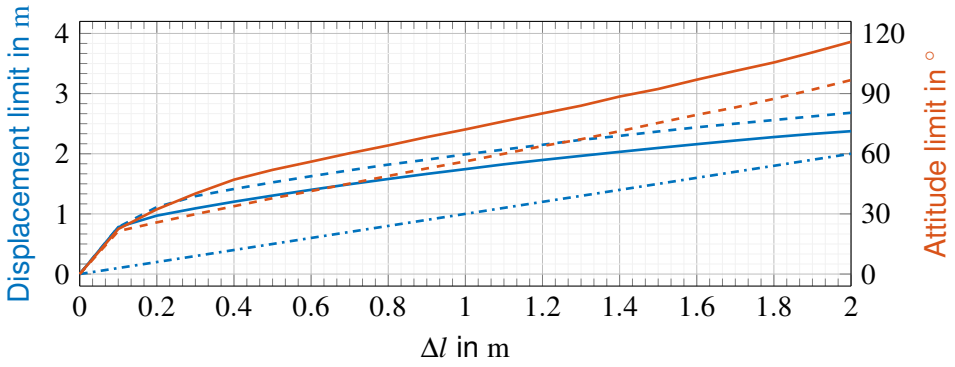


Figure 7 – Maximum axis-at-a-time deviations: translational displacement in x (——), y (- - -), and z (-·-·-), and rotational displacements in roll (——) and pitch (- - -).

data and actuator commands with a real-time SIMULINK plant model. This step verified real-time execution, I/O interfaces, and the actuator mixing logic without risking the physical aircraft.

4.4 Restrained Ground Testing

Following HIL validation, the PIXHAWK 6X was connected to the physical aircraft's actuators (PWM outputs) while the vehicle was securely restrained. A systematic verification was performed by commanding each actuator to its maximum and minimum positions in open-loop. Finally, a hover trim mission was commanded to ensure all tilt mechanisms, rotors, and control surfaces moved to their expected positions, validating the wiring and software-to-hardware mapping. Activating the different controllers enabled validation of their transient responses [16]; in the absence of pilot inputs, the resulting actuator commands should exhibit minimal deviation.

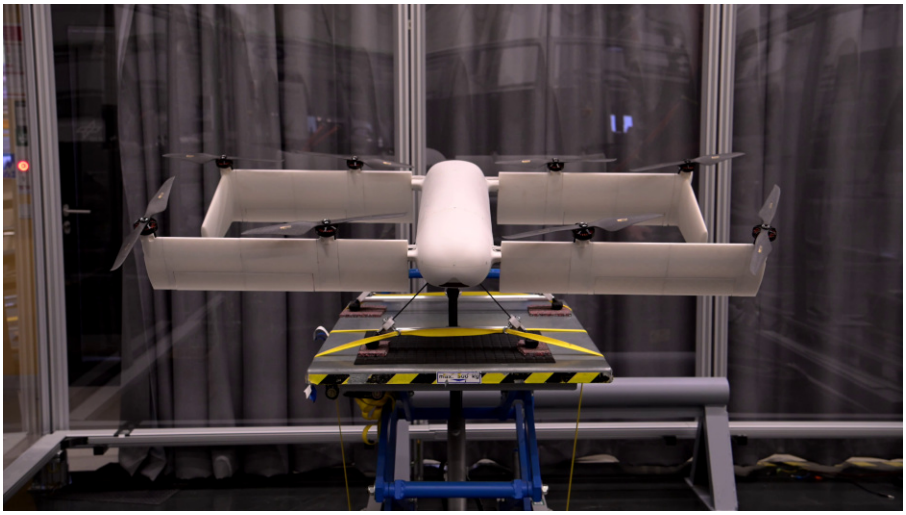


Figure 8 – Restrained Ground Testing.

5. Tethered Hover Tests and Results

The test campaign progressed through phases of an expanding flight envelope. Pre-flight fixed ground tests verified system functionality and structural integrity. Initial constraint stability checks with taut tethers evaluated both the aircraft's hover stability and tether-controller interactions as well as the dual-tether setup itself. During these tests, the direct control law was initially used to validate the hardware's sensing, actuation, and command pathways. Afterward, the baseline controller was engaged. The commands were issued by the experimental pilot via an RC transmitter. The tethers were then incrementally loosened to perform small hover maneuvers and assess control performance, stability, and disturbance rejection. During execution, the aircraft was also tethered to a ground weight to prevent uncontrolled vertical climb.

5.1 Transient Behavior and Equilibrium Hover

The initial test assesses nominal operation. The primary objective is to verify that the aircraft successfully achieves and maintains a steady-state hover equilibrium within the tethered environment without uncommanded deviations. Fig. 9 shows the transient and steady-state behavior of the aircraft during hover. The controller stabilized the aircraft within $5\,\mathrm{s}$ from a skew position. Both angles converge to their trimmed state. The pitch angle has a non-zero steady-state value because the tilt angles are not perfectly trimmed.

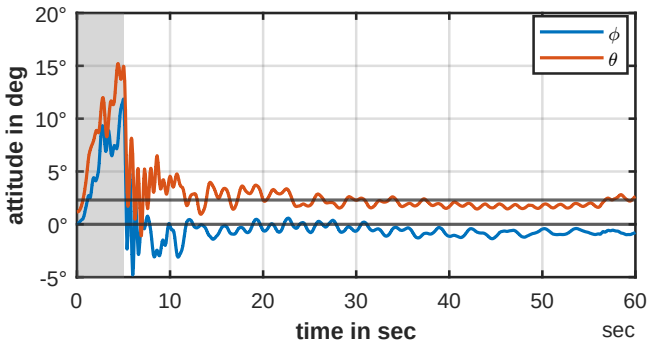


Figure 9 – Transient behavior after switching to the baseline controller. : controller inactive.

5.2 Handling of Tether Limits

To validate robustness to external constraints, the aircraft was intentionally maneuvered to its physical tether boundaries. Encountering these mechanical limits introduces unmodeled forces that act as disturbances, preventing the vehicle from reaching commanded setpoints. This testing procedure evaluates the flight controller's capacity to safely manage sudden physical constraints without destabilizing, and its ability to rapidly recover a steady-state hover equilibrium. Figure 10 shows the results of this test. The results indicate that the vehicle oscillates at the limit but does not become unstable. Furthermore, the vehicle can stabilize again after releasing the command.

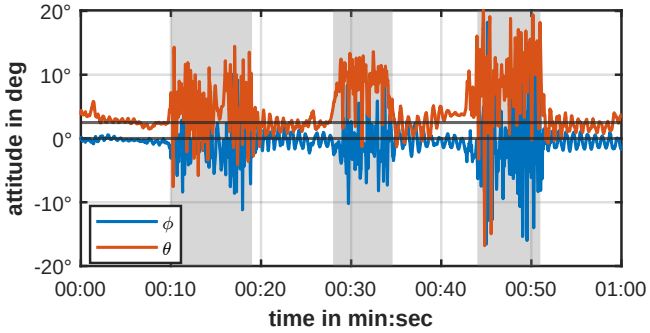


Figure 10 – Hover flight with going into the tether limits. : aircraft in tether limit.

5.3 Disturbance Rejection

To assess the flight control system's robustness to an external disturbance, a disturbance rejection test was conducted by attaching a secondary tether to the vehicle's structure. During steady-state equilibrium hover, manual tension was applied to introduce a controlled, unmodeled physical disturbance across all axes. Fig. 11 shows the aircraft's response. The baseline controller effectively mitigated this external force, successfully restoring hover equilibrium within $2\,\mathrm{s}$.

5.4 Yaw Maneuver Flight

Figure 12 illustrates the vehicle's dynamic response to a yaw rate command. The baseline controller tracked these directional commands with sufficient performance while maintaining stability across the other flight axes. The yaw maneuver induces minimal unintended deviations during hover operations.

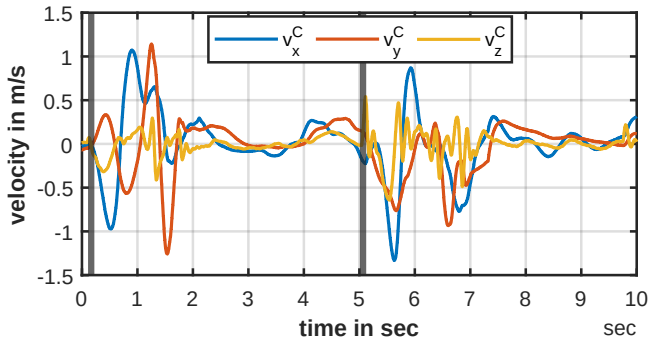


Figure 11 – System response to an external tether disturbance in hover.

This performance demonstrates yaw control and simultaneously stabilization of the roll and pitch attitude.

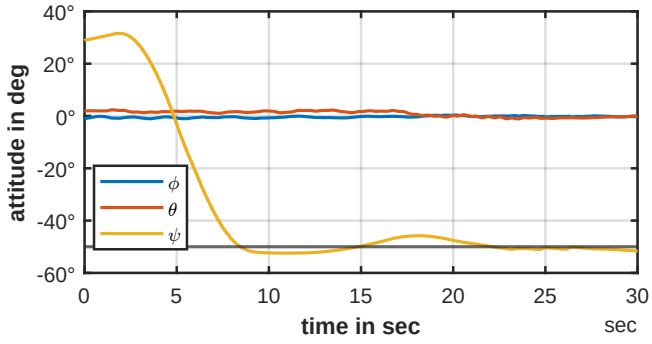


Figure 12 – Attitude response during yaw rate command tracking.

5.5 Computational Load

Finally, we evaluated whether the board's computational power is sufficient for flight control design, particularly when additional modules or control functions run concurrently in the future. The results in Fig. 13 indicate an average usage of less than one-third of the processing power and less than half of the memory limit. Therefore, when operating the system with all relevant filters and communication modules, sufficient processing capacity remains for additional or alternative control functions. Furthermore, the computational load remains stable throughout the $30\,\mathrm{min}$ flight test.

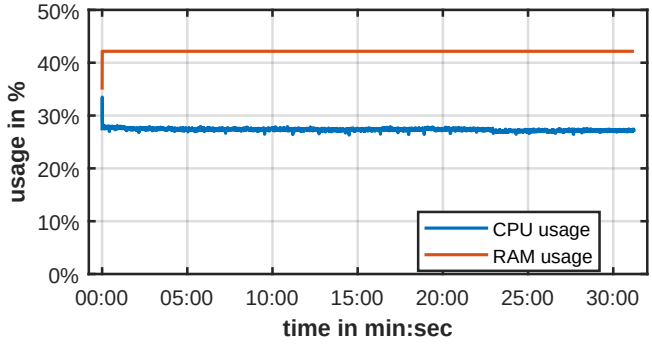


Figure 13 – CPU and RAM usage of the PIXHAWK 6X board during a $30\,\mathrm{min}$ flight test.

6. Discussion

The tethered hover tests successfully validated the baseline control laws for the *TANDEMIC* demonstrator. The aircraft achieved equilibrium with minimal steady-state errors. It also demonstrated robust disturbance rejection, recovering from external physical tether tension within $2\,\mathrm{s}$. These results establish a foundation for the broader research trajectory outlined in previous studies [1], par-

ticularly regarding the integration of advanced control architectures. The successful deployment of this baseline controller provides a safe, proven fallback system for future untethered flights. The baseline system manages over-actuation via a fixed allocation matrix. This provides a deterministic benchmark for evaluating future advanced control allocation functions. The vehicle safely navigated physical tether constraints without critical destabilization, validating the integral wind-up prevention mechanisms required for constrained flight testing. The baseline controller can serve as a stabilizing fallback in case of instability during experimental control function testing. The results of this study also help validate the overall system design, including avionics, actuators, and sensors, as well as the flight dynamics model. Hardware utilization metrics confirm an average CPU load below $33\,\%$ and RAM usage below $50\,\%$. This verifies that the flight computer has sufficient capacity to support the increased computational demands of future control laws and additional control functions.
While tethered testing isolates variables and ensures safety, mechanical constraints introduce unmodeled external forces that act as persistent disturbances, altering the vehicle's dynamic response. With the hardware, actuation pathways, and baseline stability now physically validated, future campaigns should advance the demonstrator and control laws into untethered hover tests and, ultimately, full free-flight transitions.

7. Conclusion

This paper successfully details the design, implementation, and physical validation of baseline control laws for the *TANDEMIC* tandem tilt-wing sub-scale demonstrator. Through a rigorously structured tethered hover test campaign, the implemented baseline controller demonstrated stable hover flight, effective disturbance rejection, and the ability to safely manage mechanical envelope limits without destabilizing the vehicle. Additionally, the underlying hardware and avionics architecture were validated, showing computational capacities to support the integration of more complex, advanced control algorithms in the future. By establishing this robust and deterministic fallback system, this study effectively bridges the gap between theoretical simulation and physical flight, providing the necessary foundation and confidence to safely advance the demonstrator toward untethered hover testing and eventual full free-flight transitions.

8. Contact Author Email Address

mailto: daniel.milz@dlr.de

9. Copyright Statement

The authors confirm that they, and/or their company or organization, hold copyright on all of the original material included in this paper. The authors also confirm that they have obtained permission, from the copyright holder of any third party material included in this paper, to publish it as part of their paper. The authors confirm that they give permission, or have obtained permission from the copyright holder of this paper, for the publication and distribution of this paper as part of the ICAS proceedings or as individual off-prints from the proceedings.

References

[1] D. Milz, M. May, and G. Looye. Tandem tilt-wing control law design using hybrid nonlinear dynamic inversion. *Journal of Guidance, Control, and Dynamics*, pages 1–9, 2026.

[2] M. May, D. Milz, S. F. Armanini, and G. Looye. Impact of failure on the tilt-wing evtol backward transition. *Journal of Aircraft*, 0(0):1–13, 0.

[3] P. M. Rothhaar, P. C. Murphy, B. J. Bacon, I. M. Gregory, and J. A. Grauer. Nasa langley distributed propulsion vtol tilt-wing aircraft testing, modeling, simulation, control, and flight test development. In *AIAA Aviation Technology, Integration and Operations (ATIO) Conference*, 2014.

[4] B. J. German, A. Jha, S. K. S. Whiteside, and J. R. Welstead. Overview of the research aircraft for evtol enabling technologies (raven) activity. In *AIAA Aviation 2023 Forum*, 2023.

[5] L. Ott, D. Milz, and M. May. Design and construction of a modular 3d-printed tandem tilt-wing testbed. In *AIAA SCITECH 2026 Forum*, 2026.

[6] D. D. North, R. C. Busan, and G. Howland. Design and fabrication of the la-8 distributed electric propulsion vtol testbed. In *AIAA SCITECH 2021 Forum*, 2021. AIAA Paper 2021-1188.

[7] S. C. Geuther, B. M. Simmons, and K. A. Ackerman. Overview of the subscale raven flight controls and modeling testbed. In *Vertical Flight Society 80th Annual Forum & Technology Display*, 2024.

[8] L. Panish, C. Nicholls, and M. Bacic. Nonlinear dynamic inversion flight control of a tiltwing vtol aircraft. In *AIAA SCITECH 2023 Forum*. AIAA, January 2023. AIAA Paper 2023-1910.

[9] L. Panish and M. Bacic. A generalized full-envelope outer-loop feedback linearization control strategy for transition vtol aircraft. In *AIAA AVIATION 2023 Forum*. American Institute of Aeronautics and Astronautics, June 2023.

[10] D. Enns, D. Bugajski, R. Hendrick, and G. Stein. Dynamic inversion: an evolving methodology for flight control design. *International Journal of Control*, 59(1):71–91, 1994.

[11] X. Wang, E.-J. van Kampen, Q. Chu, and P. Lu. Stability analysis for incremental nonlinear dynamic inversion control. *Journal of Guidance, Control, and Dynamics*, 42(5):1116–1129, May 2019.

[12] Y. Kumtepe, T. Pollack, and E.-J. V. Kampen. Flight control law design using hybrid incremental nonlinear dynamic inversion. In *AIAA SCITECH 2022 Forum*. American Institute of Aeronautics and Astronautics, January 2022.

[13] D. Milz, M. S. May, S. F. Armanini, and G. Looye. Stability and robustness of a tandem tilt-wing vtol with dynamic inversion control laws. In *AIAA SCITECH 2026 Forum*, 2026.

[14] P. J. Seiler, A. Packard, and P. Gahinet. An introduction to disk margins. *IEEE Control Systems*, 40:78–95, 2020.

[15] H.-D. Joos, J. Bals, G. Looye, K. Schnepper, and A. Varga. A multi-objective optimisation-based software environment for control systems design. In *Proc. of CCA/CACSD 2002*, pages 7–14, September 2002.

[16] C. Weiser, D. Milz, M. S. May, R. B. Konatala, S. J. Langen, R. Müller, C. Schreppel, and G. Looye. Flight testing advanced control functions on a passenger aircraft. In *2024 CEAS EuroGNC*, June 2024.